

Highly Linear and Stable Flexible Temperature Sensors Based on Laser-Induced Carbonization of Polyimide Substrates for Personal Mobile Monitoring

Srinivas Gandla, Muhammad Naqi, Mingoo Lee, Jung Joon Lee, Yoochan Won, Pavan Pujar, Junchul Kim, Sunghoo Lee,* and Sunkook Kim*

Wearable on-skin electronic devices that can monitor temperature in real time are of significant interest for personalized mobile health monitoring. Here, a flexible temperature sensor directly patterned by laser-induced carbonization on Kapton polyimide films integrated with flexible printed circuit boards is reported. The proposed sensor design possessing high resistance values exhibits high-linear and stable response to temperatures when integrated with flexible printed circuit boards (FPCBs) to enable continuous monitoring. The anisotropic conductive film bonding technique is used to obtain the stable real-time monitoring data under various complex environments. The sensor integration with a wearable patch based FPCB establishes conformal contacts with human skin and allows wireless sensing capabilities smoothly in real time. This kind of approach can enable multifunctional sensors to be directly laser patterned on FPCBs without any additional interfacing.

different structural forms have been synthesized to fabricate various electronic devices and sensors due to their unique functional properties. Despite its unique features, straightforward synthesis, and most importantly patterning, of high quality (high conductivity) carbon structures in a scalable approach is quite challenging. Toward this, initial groundworks have already shown promising routes to produce highly conductive carbon structures. Over the past few decades, decrease in the electrical resistivity of polymers have been reported through ion beam bombardment, pyrolysis by thermal radiation, and visible laser ablation by photo-thermal or photophysical.^[1–5] Among these, initial observations took place to

1. Introduction


Flexible electronic devices with the newly developed nano-materials through straightforward laser writing have been emerged with unique functionality. Unlike, conventional rigid electronics, flexibility offers thin, light-weight, low-cost, mechanical stability, and conformability. As of now, the most widely used unconventional substrates for flexible electronic devices include polyethylene terephthalate (PET), polyethylene naphthalate (PEN), and polyimide (PI). Among these, PI has been a strong candidate for interfacing with flexible printed circuit board electronics due to its high thermal stability, excellent mechanical stability, and dielectric properties. Thus, flexible electronics devices with PI as a substrate material have been widely reported. On the other hand, elemental carbon in

convert polyimide substrates into electrically conductive films (10^{16} to $3 \times 10^{-3} \Omega \text{ cm}$) is by ion beam bombardment in the keV range, ascribed as beam-induced carbonization, in which the chemical structure of the polymer material is forced to drastically convert into highly cross-linked carbon structures. On the other hand, pyrolysis process that undergo thermochemical decomposition of polymer material in the absence of oxygen yields carbon. Although considerable electrical resistivities down to $10^{-2} \Omega \text{ cm}$ have been achieved by these methods, they are time-consuming in the case of ion beams or have poor surface quality and inefficient to produce spatial resolution.^[6] Later, lasers have evolved to directly write desired carbon patterns on polyimide substrates without any additional process or treatment to the substrate.^[7–9] Thereafter, wide variety of lasers with different wavelengths have been studied to tune the physical and chemical properties of the PI films for various applications.^[10–18] Similarly, blending polymers or nanoparticles or doping with polyimide material or with other polymers followed by laser-induced graphene have also been reported.^[19–24] Among these, temperature sensors produced by laser-induced carbonization, more importantly exhibiting stable and linear response to temperature have not been reported yet.

The demand of real-time monitoring systems based on flexible sensors is rapidly increasing in the biomedical field specifically in the healthcare industry. As it is known that the thermoregulation system of human body maintains homeostasis boundaries and body temperature plays a vital role in human healthcare settings.^[25] A human body temperature

Dr. S. Gandla, M. Naqi, Dr. J. J. Lee, Y. Won, Dr. P. Pujar, Prof. S. Kim
Multifunctional Nano Bio-Electronics Lab
Department of Advanced Materials and Science Engineering
Sungkyunkwan University
Suwon, Gyeonggi-do 16419, South Korea
E-mail: intel0616@gmail.com

M. Lee, J. Kim, Dr. S. Lee
Korea Electronics Technology Institute (KETI)
Seongnam, Gyeonggi-do 13509, South Korea
E-mail: 2sungho@gmail.com

 The ORCID identification number(s) for the author(s) of this article can be found under <https://doi.org/10.1002/admt.202000014>.

DOI: 10.1002/admt.202000014

outside the normal range predicts a disease or its progression that requires real-time monitoring system for early diagnosis.^[26,27] Thus, a smart system is highly demanding for continuous monitoring of body temperature so that a user can take necessary steps from preventing body temperature related diseases. In addition, it is required to not only develop smart devices but also provide accurate and precise information of body temperature under complex environments.

Herein, we report a stable and highly linear temperature sensors of laser-induced carbonization of PI substrates produced by rapid bench-top nano-pulsed laser machine. The sensor exhibited temperature coefficient of resistance of $0.00142\text{ }^{\circ}\text{C}^{-1}$. The laser-induced carbonized (LIC) temperature sensor exhibits linear and stable behavior under various temperature. In addition, to verify the sensitivity of the proposed laser-induced carbonized temperature sensor the potential applications such as blowing, finger touching, breathing, and cold-hot water tests were performed. The prepared sensor shows excellent sensitivity in a short time with higher accuracy and greater stability. To assemble the smart wearable healthcare device as a conformable flexible device, the part of electronic circuit components, i.e., a customized signal processing integrated circuit (IC), a wireless communication system (Bluetooth (BLE) module), and a battery were mounted on the flexible printed circuit board (FPCB). The anisotropic conductive film (ACF) bonding technique is used to bond the proposed temperature sensor with FPCB at $200\text{ }^{\circ}\text{C}$ to obtain stable and accurate biological signals under complex environments. In addition, multilayer biocompatible patch design is utilized for attaching the smart flexible device on any part of human body for temperature monitoring. The custom-built smartphone android application is developed to provide real-time monitoring of body temperature to aid in medical checkups for patients and assist the caregiver to take necessary steps in emergency situations. This approach is rapid, scalable, and can be applicable to roll-to-roll process for mass production, thus, providing a new platform in the healthcare industry.

2. Result and Discussion

The proposed patch-based biomedical device can easily be attached on any part of human body (attached on left rib in **Figure 1a**), able to achieve accurate temperature monitoring through customized signal processing system as shown in **Figure 1a**. The proposed temperature monitoring biomedical device consists of: 1) laser-induced carbonized temperature sensor, 2) battery, 3) switch, 4) customized signal processing IC, 5) Wheatstone bridge, and (6) microcontroller with BLE module as labeled in **Figure 1a**. The entire operating system of proposed biomedical device such as amplifying, modulating, signal filtering, and transmitting the temperature signals is described in more details in the Experimental Section. The fabrication process of the proposed laser-induced carbonized temperature sensor is sequentially elaborated in **Figure 1b–g** and described in detail in the Experimental Section. The temperature sensor is designed to have circular patterns for highly resistive and stable temperature sensors. The patterned sensor exhibited a high resistance of $200\text{ k}\Omega$, essential for low-power consumption. In addition, the test setup was organized to

configure the power consumption of laser-induced carbonized temperature sensor, described in Section S1 (Supporting Information). The scanning electron microscopy (SEM) image pertaining to the optimized laser parameters is shown in **Figure S1** (Supporting Information). The sensor processed by mask-less programmable bench-top laser machine ensures rapid fabrication of the sensor for low-cost wearable electronic devices.^[28] Straightforward synthesis of high-quality graphene by facile laser carbonization technique for various applications has been reported recently.^[10–18,29–35] Moreover, different lasers with different wavelengths have been applied to demonstrate various applications like sound, strain, urea, and gas sensors. For real-time monitoring of proposed temperature sensor, a patch-based biomedical device was mounted on the human body for more than 7 h as described in **Figure 1h**, distinguished by open state and attached to body. The results explain stable and accurate real-time monitoring of body temperature through the presented smart biomedical device.

Raman spectroscopy for the characterization of laser-treated PI films was carried out to know the structural information, as well as defects and disorders introduced during the laser carbonization process. Raman spectra of the laser carbonized film with the optimized laser parameters are shown in **Figure 2a**. The spectra of the laser-treated PI films exhibited two main dominant peaks (D and G peaks), around ≈ 1350 and $\approx 1580\text{ cm}^{-1}$, respectively. The D band originates from a hybridized vibrational mode related to the disordered sp^2 -hybridized graphitic structures and indicates the presence of defects in the system. Also, the G peak represents a graphite-derived structure and while 2D peak at $\approx 2700\text{ cm}^{-1}$ resulting from second-order resonance indicating complete graphitization of PI film. From **Figure 2a**, it is observed that the optimized carbonized films showed two peaks (G and D) with a broad 2D peak suggesting that the films are more likely to be glass-like carbon.^[36] However, the $I_{\text{D}}/I_{\text{G}}$ ratio confirms the crystalline nature of the optimized laser ablated surface.^[37] X-ray diffraction (XRD) was conducted to know the crystal structure of the ablated surface (**Figure 2b**). It is evident that a prominent peak is observed at $2\theta = 26^{\circ}$, representing the graphitic (002) crystal planes. This gives an interlayer spacing (d -spacing) of $\approx 3.4\text{ \AA}$, well matched with the graphitic phase, calculated using Bragg's diffraction. A (100) peak at $\approx 43^{\circ}$ and (004) peak at 53.2° are also shown, which are commonly present in graphitic carbons reflection. Moreover, the XRD data of the ablated PI films suggest that glassy carbon with layers of graphite-like microcrystallites are connected to one another by randomly misaligned regions.^[38–40] Unlike glassy carbon having strong sp^2 graphitization, amorphous carbon has a tendency of sp^3 hybridization with disorder in atomic scale. X-ray photoelectron spectroscopy (XPS) data for high-resolution C 1s, N 1s, and O 1s peaks were obtained for the polyimide substrate before and after laser treatment. Full scan of the XPS data and table providing the atomic concentrations of the polyimide substrate before and after laser treatment is depicted in **Figure S2a–c** (Supporting Information). To understand the effect of laser carbonization, the spectra were deconvoluted using a Gaussian–Lorentzian decomposition into individual peaks for further analysis. It was found that carbon containing species at binding energies: C=C/C–C/C–H at 284 eV , C–N at 285 eV , C–O at 286 eV , and C=O at 287 eV were determined (**Figure 2c,e**).

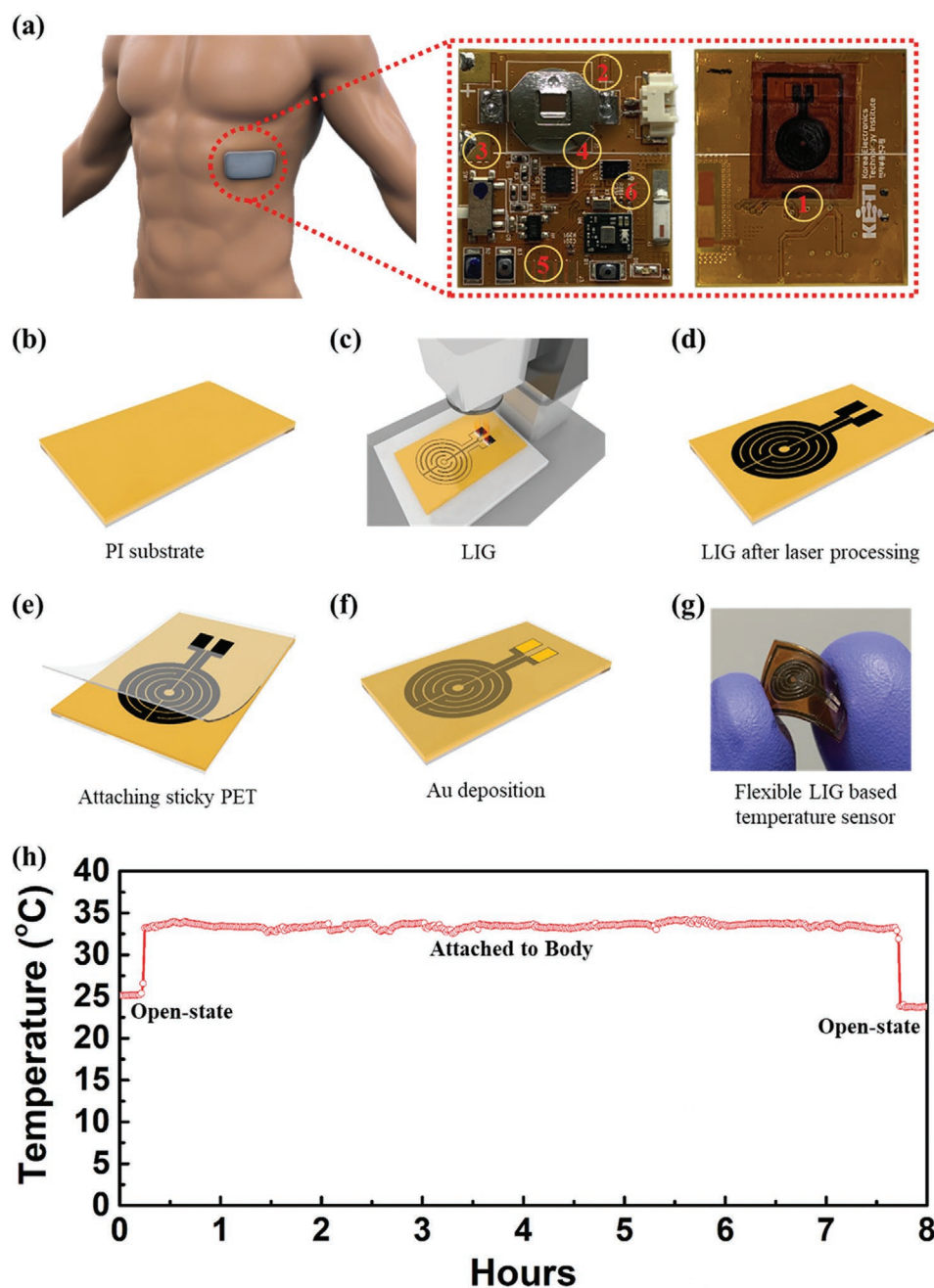


Figure 1. A concept and fabrication process of proposed LIG based temperature sensor. a) Patch-based biomedical device attached on left rib of human body (left side) and real image of flexible printed circuit board (FPCB) layout along with proposed temperature sensors (right side). b–g) Sequential fabrication process of laser-induced carbonized temperature sensor. h) Real-time monitoring data information of body temperature while attached to human body up to 7.5 h.

Similarly, oxygen and nitrogen containing species at binding energies: aromatic (C=O) at 530 and aromatic ether group (C–O–C) at 532.5 eV for oxygen, and amide 399 eV for nitrogen were detected, see Figure 2d and Figure S2d (Supporting Information). Compared to the original PI films, the peaks obtained for laser-treated samples showed a considerable increase in the C–C peak, while decrease in C=O, C–O–C, and C–N bonds, representing that the laser is able to break the carbon-related bonds of the untreated PI films and while the others nitrogen

and oxygen are escaped as gases. Also, oxygen content is significantly decreased, which is generally observed in laser carbonized PI films. So, it can be understood that the carbon-related compounds of the PI film significantly break down to produce a large content of carbon. Moreover, the ablated films dominated by sp^2 -carbons are in agreement with the Raman and XRD data.

Temperature sensors for monitoring human body thermoregulations are of significant interest for healthcare applications. Toward this, various temperature sensors with carbon-based

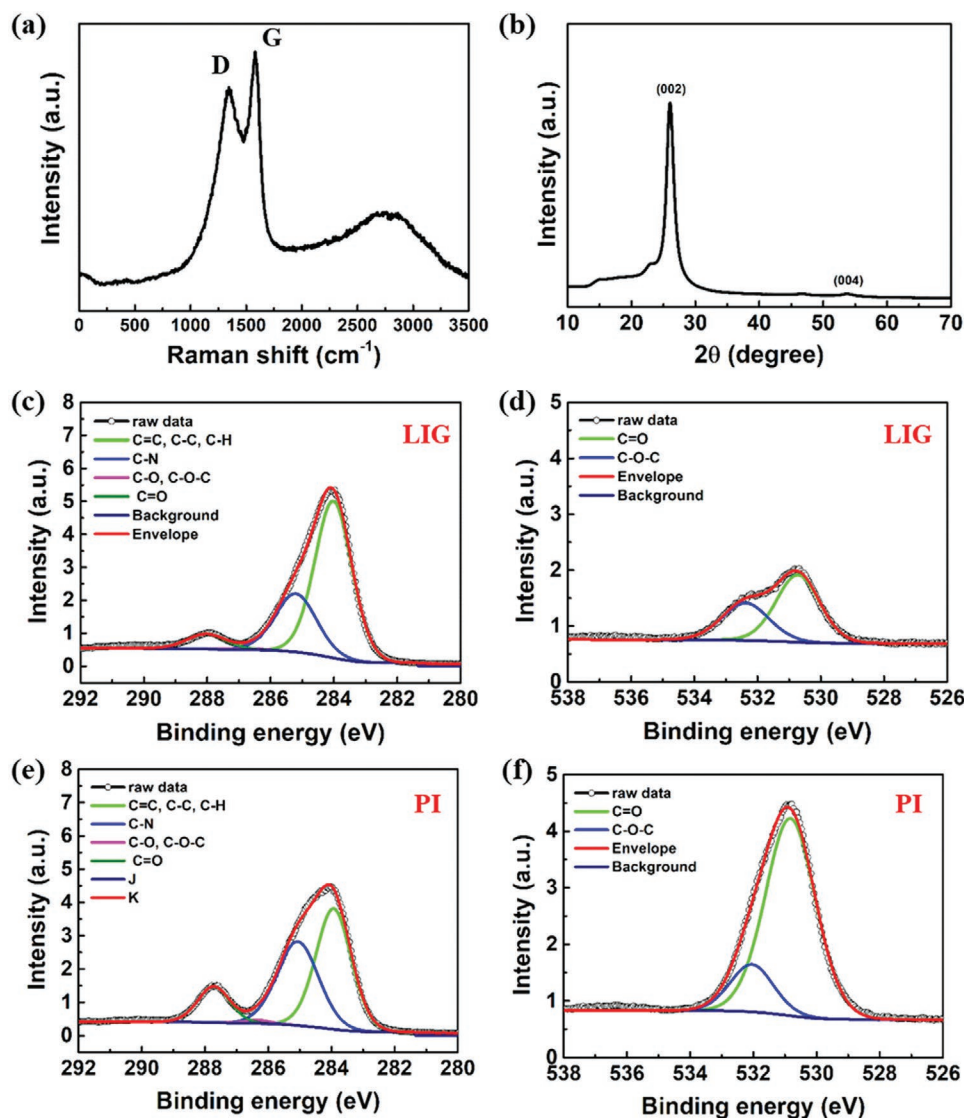


Figure 2. Material characterization of proposed temperature sensor. a) Raman spectroscopy analysis and b) X-ray diffraction (XRD) analysis of laser-induced carbonized temperature sensor. X-ray photoelectron spectroscopy (XPS) analysis of carbon and oxygen in c,d) laser induced carbonized film and e,f) pristine polyimide (PI) film.

materials as a sensing layer have been widely adopted.^[41–48] For that reason, laser-patterned carbonized films are applied to demonstrate a stable and highly linear temperature sensor. The temperature sensing of the proposed sensor was measured over the temperature range of -10 to 60 °C, exhibiting broad temperature sensing behavior including human skin temperatures, as shown in Figure 3a. The sensor exhibited a negative temperature coefficient of resistance (NTCR) of value 0.00142 °C⁻¹ with high linear ($R^2 = 0.999$) and stable responses. It was observed that the sensor was stable at all the temperature -10 to 60 °C (with 5 °C of intervals) for 10 min, shown in Figure 3b. The proposed temperature sensor was measured over the range of temperature from 30 to 46 °C (with 2 °C of interval) which is quite enough for human body temperature range, described in Figure 3c. The normalized resistance response of the sensor exhibited stable linear characteristics. Herein, the normalized resistance is defined as $\Delta R/R_0 = R_0 - R/R_0$,

where R represents the resistance value at various temperature (30 – 46 °C) and R_0 represents the resistance value at a reference temperature of 30 °C. To verify the proposed temperature sensor response, the temperature value was fluctuated from 40 to 30 °C (with an interval of 3 min) for 18 min (Figure 3d). Due to stability and high linearity of the proposed sensor, which is large enough to operate as a temperature sensor using a prepossessing block such as an amplifier and an analog-to-digital converter. After prepossessing, the accuracy of the measured temperature becomes ± 0.2 °C from 30 to 40 °C in a vacuum chamber and which is same as that of the most widely used commercial temperature sensors, namely, SHT2x, DM6801B, and wireless thermometer (WT702, raiing). Thus, the performance proposed temperature sensor is comparable to the commercial ones. Additionally, resistive-based sensors that are mostly pressure sensitive and moisture dependent are now need to be carefully addressed, because motion artifacts and moisture levels from the body

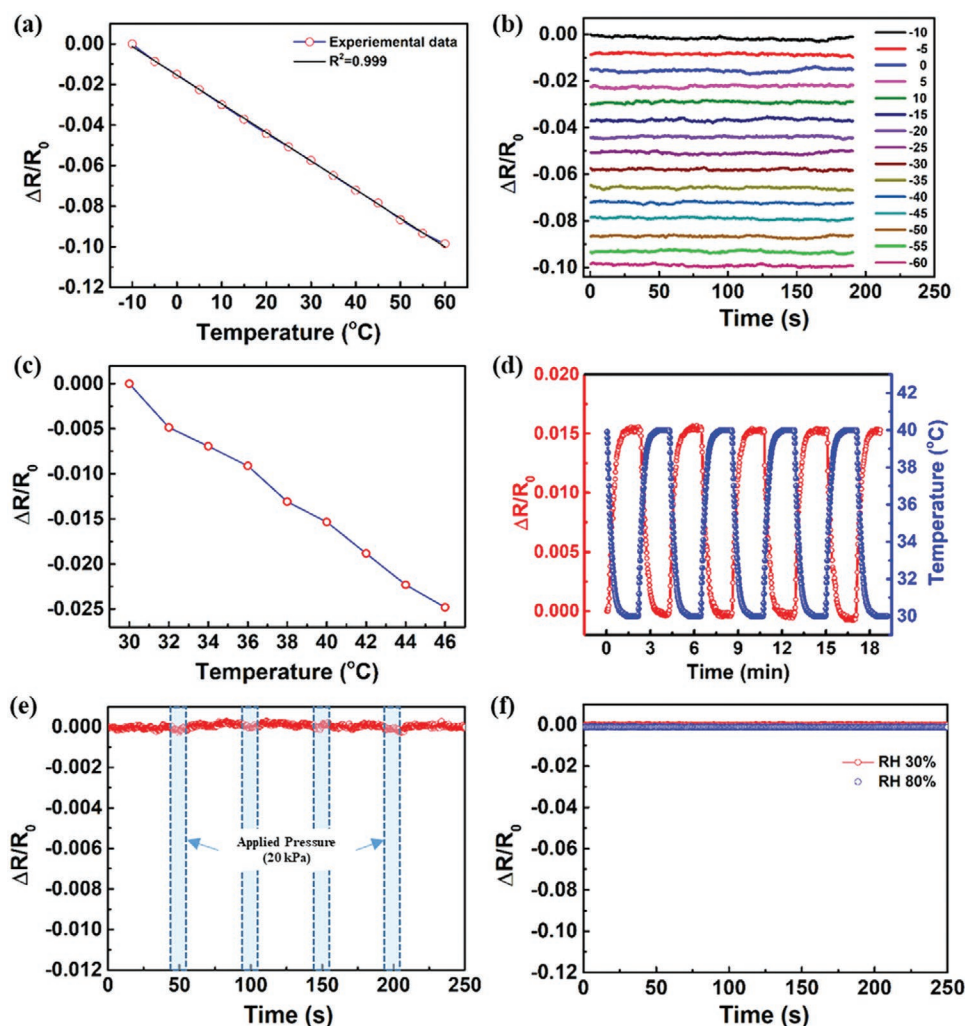


Figure 3. Electrical characterization of proposed temperature sensor. a) Normalized resistance measurements under different temperature ranges from -10 to 60 °C (with interval of 5 °C). b) The sensor's stability test from -10 to 60 °C with an interval 5 °C for 10 min. c) The resistance variations of temperature sensor ranges from 30 to 46 °C (with interval of 2 °C). d) The sensor response behavior at temperature fluctuation from 30 to 40 °C with an interval of 3 min at each temperature up to 18 min. e) The pressure dependency test by applying pressure of 20 kPa at constant temperature of 20 °C. f) Effect of humidity on resistance variation.

and environmental conditions during day-to-day life physical activities may alter the temperature values of the sensor. So, the qualitative information of the temperature can be ambiguous. A pressure (20 kPa) was applied to the sensor at fixed temperature of 20 °C and there was no significant change in resistance (Figure 3e). Moreover, the sensor exposed to pressure and humidity depicted a negligible change in resistance (Figure 3f). Even though, a slight humidity-dependent sensor performance was shown, but the relative change in resistance ($\Delta R/R_0$) for rise in relative humidities from 30% to 80% , are well below than, the relative change in resistance for 1 °C raise in temperature. In other words, even if the body temperature and humidity are simultaneously increased by 2 °C (minimum deviation) and RH 50% (maximum), the error in temperature measured due to the change in humidity can be ± 0.8 °C. In addition, the proposed temperature sensor for real-time monitoring of body temperature needs to be capable of high flexibility to obtain accurate and precise measurements under complex environments. For that,

the cyclic bending test of proposed temperature was performed up to 5000 cycles with radius of curvature 5 mm and results show a stable behavior during the experiment (Figure S3, Supporting Information).

On the other hand, the sensor was displayed to detect and monitor various human health related activities. The breath monitoring is presented in Figure 4a. The sensor was attached to the gas mask with the aid of double-sided tape and it is clearly seen that as the subject start to breathe in and out, a general trend of increase and decrease of resistance is monitored with the resistance reaching a steady state as the breathing stopped immediately. Also, when hot and cold water were dropped followed by removal on top of the encapsulated PET covering the sensor, exhibited response time of ≈ 1 s for sensing and ≈ 20 s for reaching a steady state, as shown in Figure 4b. Besides few seconds response time of the proposed sensor, sensors exhibiting millisecond response time have also been reported.^[49,50] Similarly, sensor sensitive to touching with finger and blowing

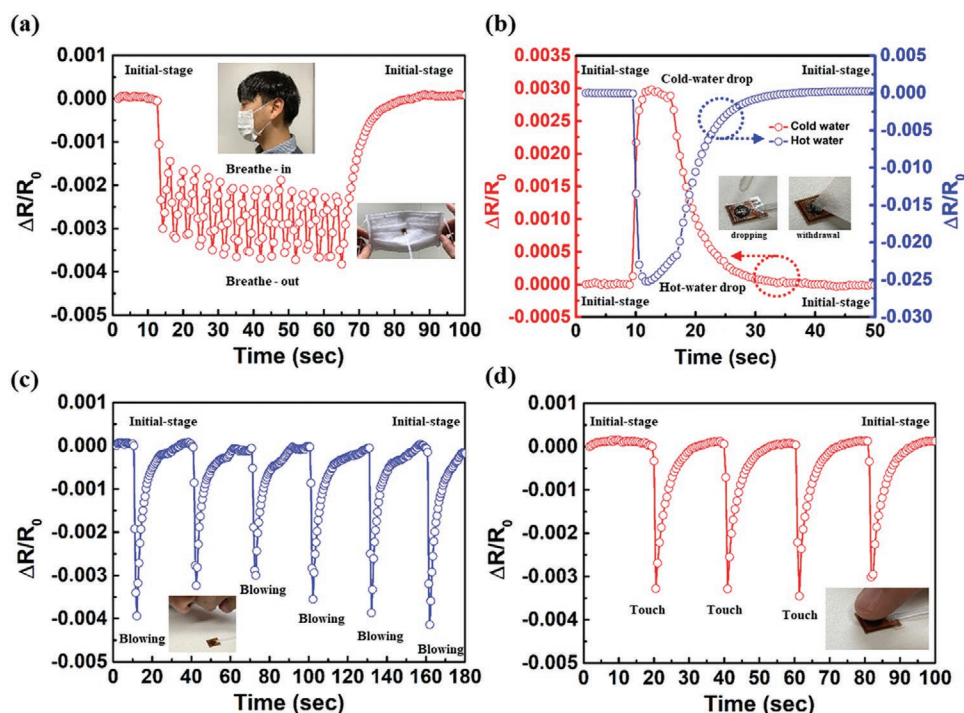


Figure 4. Some other application tests of proposed temperature sensor. a) Breath monitoring test while the sensor's attached to the lab mask. b) Hot and cold water drop test performed by simply dropping the hot and cold water drops on the sensor. c) Blowing test was performed by simply blowing on the sensor. d) Finger touch test was performed by simply touching the sensor at the top, with inset images shown in each case.

by mouth was also shown in Figure 4c,d, respectively. Images pertaining to each application are provided as an inset in Figure 4. These applications demonstrate that the proposed temperature is qualified not only for body temperature measurements but also for other healthcare industrial applications.

The underlying temperature sensing mechanism of the proposed sensor can be understood and verified through various carbon-based materials showing NTCR behaving like semiconducting properties. The charge transport in sensors exhibiting NTCR include reduced graphene oxide (rGO) and multiwall CNT is mainly governed by the semiconducting properties of the interlayered hexagonal carbon structures verified through experimental and theoretical analysis. During thermal excitation, the charge carriers jump either from the impurity/defect states to conduction band or valence band depending on the location of defect levels, which leads to decrease in resistance. Increase in electrical conductivity can also be understood by hopping and tunneling of charge carrier transport between neighboring rGO sheet to sheet, thereby, overcome the barrier potentials.^[48,51,52] Effect of lattice vibrational properties on electrical conductivity while considering charge carrier scattering within the rGO flakes has also been reported.^[45] Apart from the conduction of charge carriers, electron–phonon scattering, impurities, defects, and edges of flakes are the primary contributions in their own dynamics. Because, the phonons being heat carriers play a key role during heat transportation. During thermal excitation, the unhybridized π electrons in the sp^2 hybridized hexagonal lattice of the disorder graphene are scattered by both thermally generated charge carriers and phonons. These scatterings are temperature dependent in which variable

range hopping and electron–phonon scattering mechanisms are dominant at low temperature and high temperature.^[47] Based on these mechanisms, the temperature sensing of defective glass-like carbon structures that possess disordered crystalline domains of sp^2 hybridized hexagonal structures exhibiting NTCR can be interpreted similar to that of a semiconductor type. For the cases of sensor response above 300 K is analyzed with the Arrhenius equation (R – T relation), expressed as: $R(T) = R_0 \exp(-E_g/k_B T)$, where R is the resistance at certain temperature T , R_0 is the resistance at initial temperature, E_g is the activation energy, and k is the Boltzmann constant. The activation energy obtained for the curve plotted with $\ln(R)$ versus $1000/T$ is ≈ 9 meV and which is low compared to that of the previous reports (Figure S4, Supporting Information).^[45,47,52–55] The reason for low activation energy might be due to thermally excited free charge carriers in case of the glass-like carbon structures, which are mainly scattered by defects, edge of domains, and electron–phonon interactions.^[56,57] The crystallites of the carbon being smaller in size (≈ 4.52 nm) contribute to the large grain boundary area thereby enhanced scattering of the charge carriers. Therefore, restricts the effective way of increasing charge carrier transport through tunneling process. Moreover, previous studies on the glassy carbon structures suggest a similar behavior of resistance versus temperature.^[56]

Overall, with the advantages obsessed by the laser carbonization technique, the highly linear and stable temperature sensor has been applied to demonstrate a wearable patch-based sensor to deliver real-time temperature information to the personalized smartphone. A wearable patch-based smart device is attached to the right arm of human body as shown

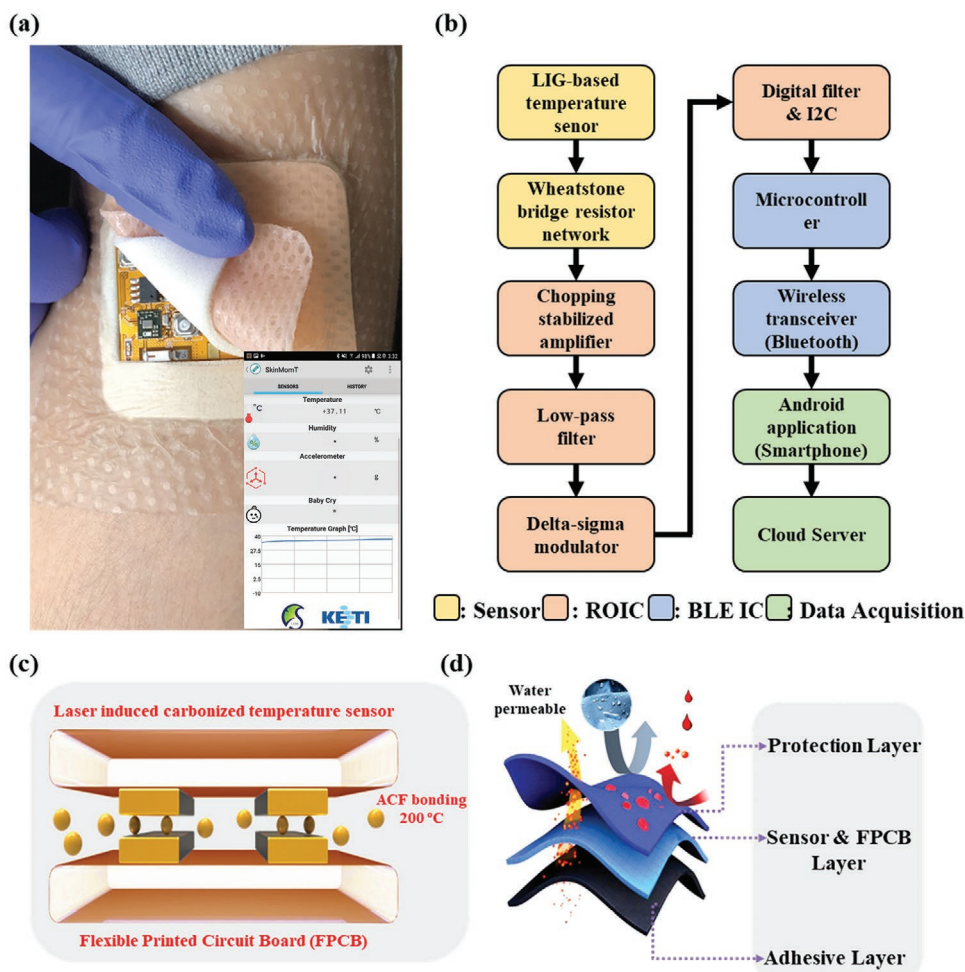


Figure 5. Operating system and patch design of proposed biomedical device. a) The proposed biomedical device attached to the human body (left arm) and inset is the customized android application. b) Flowchart of entire operating system for data acquisition from proposed temperature sensor. c) Bonding mechanism of sensor and FPCB modules by ACF bonding method. d) Patch design layout of the proposed biomedical device.

in **Figure 5a** and the custom-built android application is elaborated in the inset of **Figure 5a** which displays the real-time data stream of temperature monitoring. The entire operating system of proposed biomedical device is described in the flowchart in **Figure 5b**, elaborating the process in following way: 1) First, the analog signals obtained from laser-induced carbonized temperature sensor amplified by chopping stabilized amplifier after passing the signals from Wheatstone bridge resistive network, 2) to filter the noises from the amplified signals of temperature sensor, a low-pass filter was used, 3) the filtered analog signals then digitized using 16-bit delta-sigma modulator, and 4) the digitized biological signals then wirelessly transmitted via BLE module and stored in cloud server simultaneously. The performance of the signal-to-noise ratio through the signal measuring path is limited to 50 dB, which is enough to display the temperature data with the targeted accuracy and the range (± 0.2 °C from 30 to 40 °C). In addition, the structure of measuring electronics is described in **Figure S5** (Supporting Information). To obtain strong bonding between proposed temperature sensor and FPCB, ACF bonding technique has been introduced which operates at 200 °C to provide accurate and precise information

of body temperature (**Figure 5c**). The wearable patch possessing adhesion, breathable, and water absorbing layers ensures conformal contacts to skin without producing any adverse effects. At the same time, continuous monitoring of temperature is also essential before the FPCB battery gets drained out. For that reason, the patch of temperature sensor is designed in three layers: 1) protection layer made up of hydrophilic polyurethane film that protects human skin and device module, 2) sensor and FPCB layer consists of proposed temperature sensor and device module to obtain biological signals with high accuracy, and 3) adhesive layer which is able to absorb moisture obtained from human body and attach to human skin conformally (**Figure 5d**).

3. Conclusion

Rapid manufacturing of highly stable and linear flexible temperature sensor via laser-induced carbonization capable of delivering real-time monitoring of human skin temperature through wireless for mobile healthcare applications was proposed in this study. The sensor exhibited quick responses to

human activities that are necessary for health-related subjects. Due to high stability and linearity, the temperature equivalent digital processing is straightforward and therefore was able to realize sensor for practical applications. The facile fabrication of LIC-based temperature sensors can enable other potential applications compatible with traditional FPCBs.

4. Experimental Section

Sensor Fabrication: Commercially available Kapton (PI) sheets with thickness of 125 μm were purchased and used as received without any additional treatments to the surface. Small pieces of PI were cut into an appropriate dimension and cleaned with IPA in an ultrasonicator. The cleaned PI substrates were rinsed with deionized (DI) water for three times and then subjected to a laser carbonization. A bench-top programmable laser machine (INLASER, Korea) with a wavelength of 1064 nm which costs $\approx 28\,000$ \$ was used in this process. No additional steps were involved for setup to fabricate the sensor. The overall process time to fabricate the sensor was achieved within few minutes and mainly depends on the size of the sensor. Desired patterns were designed in AutoCAD, which were then later fed into the laser machine to form carbon traces within the surface of the PI substrate. Mask-less laser-induced carbonization procedure is schematically illustrated in Figure 1b–g. The laser beam size, frequency, and scanning speed are 20 μm , 100 kHz, and 500 mm min^{-1} . After the laser irradiation, Au of 100 nm thickness was deposited by E-beam by placing shadow mask aligning the carbonized contact pads. Finally, the substrate was encapsulated with sticky PET to avoid interaction with environment moieties.

Material Characterization: Microscopic images of the laser carbonized substrates were obtained by Olympus Microscope. X-ray diffraction was performed using SmartLab, Rigaku Corp. Raman spectroscopy and XPS were carried out by using WITec confocal raman, alpha 300 R, and ThermoFisher Scientific, K-Alpha⁺, respectively.

Electrical and Mechanical Measurements: Electrical current–voltage (I – V) was carried out by Keithley 4200-SCS where the temperature was controlled via hot chuck controller (HCC) system and mechanical measurements were carried out by ultimate tensile machine (UTM) Mark 10 Corp. (model ESM303).

Customized Circuit Design: The proposed laser-induced carbonized temperature sensor was mounted on FPCB using ACF bonding method. For real-time monitoring of body temperature, a customized signal processing IC and readout integrated circuit (ROIC) were designed to display body temperature data stream at mobile application. For this purpose, a conventional amplifying, filtering, and digitizing technique was utilized by customizing chopping stabilized amplifier, low-pass filter, and Digital I2C interface microcontroller, respectively. To generate noise-free differential voltage signal, a Wheatstone resistive bridge network was formed for obtaining the temperature signals from proposed temperature sensor. The differential voltage signals obtained from Wheatstone bridge network was amplified by 30 dB and flicker noise was generated in amplifying process to deteriorate the temperature signals. A two-stage amplifier based on chopping stabilized amplifier was utilized to suppress the flicker noise of the amplifier. After suppressing the flicker noise, the output voltage of amplifier is defined as $V_{in} \times G_{m1}/G_{m2} \times ((R_1+2) \times R_2)/R_1$ with a reduction loop of G_{m4} and G_{m5} (Figure S6, Supporting Information). Then flicker noise was shifted to high frequency and filtered by low-pass filter. After filtering the analog signal, the temperature signals then digitized and wirelessly transmitted to the smartphone application using BLE module (SESUBPANT2541).

The experiments involving human subjects have been performed with the full, informed consent of the volunteers. To obtain preliminary data as a pilot study, the Institutional Review Boards of an affiliated university approval was obtained prior to human application (IRB no. Y-2017-0031).

Supporting Information

Supporting Information is available from the Wiley Online Library or from the author.

Acknowledgements

S.G. and M.N. contributed equally to this work. This research was supported by the National Research Foundation of Korea (2018R1D1A1B07048232). This work was supported by the Ministry of Trade, Industry, and Energy (MOTIE) and Korea Evaluation Industrial Technology (KEIT) through the Industrial Strategic Technology Development Program (10079571). This work was partly supported by the GRRC program of Gyeonggi province (GRRC Sungkyunkwan 2017-B06, Nano-biosensor based on flexible material) and Institute of Information & communications Technology Planning & Evaluation (IITP) grant funded by the Korea government (MSIT) (No. 2019-0-01303).

Conflict of Interest

The authors declare no conflict of interest.

Keywords

biomedical devices, FPCB, laser-induced carbonization, real-time monitoring, temperature sensors

Received: January 6, 2020

Revised: March 2, 2020

Published online:

- [1] G. Marletta, C. Oliveri, G. Ferla, S. Pignataro, *Surf. Interface Anal.* **1988**, 12, 447.
- [2] T. Venkatesan, S. R. Forrest, M. L. Kaplan, C. A. Murray, P. H. Schmidt, B. J. Wilkens, *J. Appl. Phys.* **1983**, 54, 3150.
- [3] H. Hatori, Y. Yamada, M. Shiraiishi, M. Yoshihara, T. Kimura, *Carbon* **1996**, 34, 201.
- [4] J. Davenas, *Appl. Surf. Sci.* **1989**, 36, 539.
- [5] C. Decker, *J. Polym. Sci., Part C: Polym. Lett.* **1987**, 25, 5.
- [6] M. Schumann, R. Sauerbrey, M. C. Smayling, *Appl. Phys. Lett.* **1991**, 58, 428.
- [7] R. Srinivasan, R. R. Hall, W. D. Wilson, W. D. Loehle, D. C. Allbee, *Chem. Mater.* **1994**, 6, 888.
- [8] R. Srinivasan, R. R. Hall, D. C. Allbee, *Appl. Phys. Lett.* **1993**, 63, 3382.
- [9] R. W. Dreyfus, *Appl. Phys. A: Solids Surf* **1992**, 55, 335.
- [10] R. Rahimi, M. Ochoa, W. Yu, B. Ziaie, *ACS Appl. Mater. Interfaces* **2015**, 7, 4463.
- [11] L.-Q. Tao, H. Tian, Y. Liu, Z.-Y. Ju, Y. Pang, Y.-Q. Chen, D.-Y. Wang, X.-G. Tian, J.-C. Yan, N.-Q. Deng, Y. Yang, T.-L. Ren, *Nat. Commun.* **2017**, 8, 14579.
- [12] C. M. Tittle, D. Yilman, M. A. Pope, C. J. Backhouse, *Adv. Mater. Technol.* **2018**, 3, 1700207.
- [13] L. X. Duy, Z. Peng, Y. Li, J. Zhang, Y. Ji, J. M. Tour, *Carbon* **2018**, 126, 472.
- [14] B. Sun, R. N. McCay, S. Goswami, Y. Xu, C. Zhang, Y. Ling, J. Lin, Z. Yan, *Adv. Mater.* **2018**, 30, 1804327.
- [15] M. R. Bobinger, F. J. Romero, A. Salinas-Castillo, M. Becherer, P. Lugli, D. P. Morales, N. Rodríguez, A. Rivadeneyra, *Carbon* **2019**, 144, 116.

- [16] D. X. Luong, K. Yang, J. Yoon, S. P. Singh, T. Wang, C. J. Arnsch, J. M. Tour, *ACS Nano* **2019**, *13*, 2579.
- [17] M. G. Stanford, K. Yang, Y. Chyan, C. Kittrell, J. M. Tour, *ACS Nano* **2019**, *13*, 3474.
- [18] E. R. Mamleyev, S. Heissler, A. Nefedov, P. G. Weidler, N. Nordin, V. V. Kudryashov, K. Länge, N. MacKinnon, S. Sharma, *NPJ Flexible Electron.* **2019**, *3*, 2.
- [19] R. Ye, Z. Peng, T. Wang, Y. Xu, J. Zhang, Y. Li, L. G. Nilewski, J. Lin, J. M. Tour, *ACS Nano* **2015**, *9*, 9244.
- [20] A. Z. Yazdi, I. O. Navas, A. Abouelmagd, U. Sundararaj, *Macromol. Rapid Commun.* **2017**, *38*, 1700176.
- [21] Z. Peng, R. Ye, J. A. Mann, D. Zakhidov, Y. Li, P. R. Smalley, J. Lin, J. M. Tour, *ACS Nano* **2015**, *9*, 5868.
- [22] R. Ye, X. Han, D. V. Kosynkin, Y. Li, C. Zhang, B. Jiang, A. A. Martí, J. M. Tour, *ACS Nano* **2018**, *12*, 1083.
- [23] L. Ge, Q. Hong, H. Li, F. Li, *Chem. Commun.* **2019**, *55*, 4945.
- [24] A. K. Thakur, S. P. Singh, M. N. Kleinberg, A. Gupta, C. J. Arnsch, *ACS Appl. Mater. Interfaces* **2019**, *11*, 10914.
- [25] A. Rahali, M. Guerbaoui, A. Ed-dahhak, Y. El Afou, A. Tannouche, A. Lachhab, B. Bouchikhi, *Int. J. Eng., Sci. Technol.* **2012**, *3*.
- [26] S. Lee, H. Kim, M. G. Lee, S. Kim, S. Gandla, M. Naqi, U. Jung, S. Kang, H. S. Yoon, D. G. Pyun, Y. Lee, H.-J. Kwon, *IEEE Trans. Ind. Electron.* **2019**, *1*.
- [27] S.-O. Yun, J. H. Lee, J. Lee, C.-Y. Kim, *IEICE Trans. Inf. Syst.* **2019**, *E102.D*, 1115.
- [28] H. Chae, H.-J. Kwon, Y.-K. Kim, Y. Won, D. Kim, H.-J. Park, S. Kim, S. Gandla, *ACS Appl. Mater. Interfaces* **2019**, *11*, 28387.
- [29] J. Kim, J.-H. Jeon, H.-J. Kim, H. Lim, I.-K. Oh, *ACS Nano* **2014**, *8*, 2986.
- [30] Q. Wang, Y.-T. Li, T.-Y. Zhang, D.-Y. Wang, Y. Tian, J.-C. Yan, H. Tian, Y. Yang, F. Yang, T.-L. Ren, *Appl. Phys. Lett.* **2018**, *112*, 133902.
- [31] T.-Y. Zhang, Q. Wang, N.-Q. Deng, H.-M. Zhao, D.-Y. Wang, Z. Yang, Y. Liu, Y. Yang, T.-L. Ren, *Appl. Phys. Lett.* **2017**, *111*, 121901.
- [32] G. F. Hawes, D. Yilman, B. S. Noremberg, M. A. Pope, *ACS Appl. Nano Mater.* **2019**, *2*, 6312.
- [33] Y.-Q. Liu, Z.-D. Chen, J.-W. Mao, D.-D. Han, X. Sun, *Front. Chem.* **2019**, *7*, 461.
- [34] P. Peng, L. Li, P. He, Y. Zhu, J. Fu, Y. Huang, W. Guo, *Nanotechnology* **2019**, *30*, 185301.
- [35] Y. Li, D. X. Luong, J. Zhang, Y. R. Tarkunde, C. Kittrell, F. Sargunraj, Y. Ji, C. J. Arnsch, J. M. Tour, *Adv. Mater.* **2017**, *29*, 1700496.
- [36] J. Lin, Z. Peng, Y. Liu, F. Ruiz-Zepeda, R. Ye, E. L. G. Samuel, M. J. Yacaman, B. I. Yakobson, J. M. Tour, *Nat. Commun.* **2014**, *5*, 5714.
- [37] L. G. Caçado, K. Takai, T. Enoki, M. Endo, Y. A. Kim, H. Mizusaki, A. Jorio, L. N. Coelho, R. Magalhães-Paniago, M. A. Pimenta, *Appl. Phys. Lett.* **2006**, *88*, 163106.
- [38] M. I. Nathan, J. E. Smith, K. N. Tu, *J. Appl. Phys.* **1974**, *45*, 2370.
- [39] X. J. Gu, *Appl. Phys. Lett.* **1993**, *62*, 1568.
- [40] K. Jurkiewicz, M. Pawlyta, A. Burian, *C* **2018**, *4*, 68.
- [41] M. Tian, Y. Huang, W. Wang, R. Li, P. Liu, C. Liu, Y. Zhang, *J. Mater. Res.* **2014**, *29*, 1288.
- [42] Y. Khan, M. Garg, Q. Gui, M. Schadt, A. Gaikwad, D. Han, N. A. D. Yamamoto, P. Hart, R. Welte, W. Wilson, S. Czarnecki, M. Poliks, Z. Jin, K. Ghose, F. Egitto, J. Turner, A. C. Arias, *Adv. Funct. Mater.* **2016**, *26*, 8764.
- [43] B. Davaji, H. D. Cho, M. Malakoutian, J.-K. Lee, G. Panin, T. W. Kang, C. H. Lee, *Sci. Rep.* **2017**, *7*, 8811.
- [44] M. Marengo, G. Marinaro, J. Kosel, in *2017 IEEE SENSORS*, IEEE, Piscataway, NJ **2017**, pp. 1–3.
- [45] P. Sehwat, Abid, S. S. Islam, P. Mishra, *Sens. Actuators, B* **2018**, *258*, 424.
- [46] G. Liu, Q. Tan, H. Kou, L. Zhang, J. Wang, W. Lv, H. Dong, J. Xiong, *Sensors* **2018**, *18*, 1400.
- [47] A. Kaur, R. C. Singh, *J. Mater. Sci.: Mater. Electron.* **2019**, *30*, 5791.
- [48] Q. Liu, H. Tai, Z. Yuan, Y. Zhou, Y. Su, Y. Jiang, *Adv. Mater. Technol.* **2019**, *4*, 1800594.
- [49] T. Yokota, Y. Inoue, Y. Terakawa, J. Reeder, M. Kaltenbrunner, T. Ware, K. Yang, K. Mabuchi, T. Murakawa, M. Sekino, W. Voit, T. Sekitani, T. Someya, *Proc. Natl. Acad. Sci. USA* **2015**, *112*, 14533.
- [50] S. Mandal, M. Banerjee, S. Roy, A. Mandal, A. Ghosh, B. Satpati, D. K. Goswami, *ACS Appl. Mater. Interfaces* **2019**, *11*, 4193.
- [51] C. Gómez-Navarro, R. T. Weitz, A. M. Bittner, M. Scolari, A. Mews, M. Burghard, K. Kern, *Nano Lett.* **2007**, *7*, 3499.
- [52] A. Tewari, S. Gandla, S. Bohm, C. R. McNeill, D. Gupta, *FlatChem* **2019**, *16*, 100110.
- [53] P. Sahatiya, S. K. Puttapati, V. V. S. S. Srikanth, S. Badhulika, *Flexible Printed Electron.* **2016**, *1*, 025006.
- [54] I. Banerjee, T. Faris, Z. Stoeva, P. G. Harris, J. Chen, A. K. Sharma, A. K. Ray, *2D Mater.* **2016**, *4*, 015036.
- [55] S. Kanaparthi, S. Badhulika, *Nanotechnology* **2016**, *27*, 095206.
- [56] D. F. Baker, R. H. Bragg, *J. Non-Cryst. Solids* **1983**, *58*, 57.
- [57] L. A. Pesin, *J. Mater. Sci.* **2002**, *37*, 1.